

The Assessment of Ankle Osteoarthritis with Weight-Bearing Computed Tomography

Martinus Richter, MD, PhD^{a,b,*}, Cesar de Cesar Netto, MD^{a,c},
Francois Lintz, MD^{a,d}, Alexej Barg, MD^{a,e}, Arne Burssens, MD^{a,f},
Scott Ellis, MD^{a,g}

KEYWORDS

• Ankle • Osteoarthritis • Weight-bearing CT • WBCT • Alignment

KEY POINTS

- The cone beam technology as such is similar to previous applications as for example intra-operative 3D-imaging.
- The accuracy of the bone position assessment, i.e. different measurement of angles between bones or position of bones have been investigated in many studies.
- The assessment of the hindfoot axis, position of the fibula in relation to the tibia and joint space analysis are important for the assessment of ankle osteoarthritis (AOA) and for treatment planning.

INTRODUCTION

Weight-Bearing CT (WBCT) was not especially invented for the assessment of ankle osteoarthritis (AOA). The principles of the technology and the evolvement of use are also the basis for the assessment of AOA as described in the following. The standard for diagnostic radiographic imaging in foot and ankle surgery was until 2012 radiographs with full weight-bearing without any useful alternative.¹⁻³ The three-dimensional position of bones and relationships between bones in the foot (for example angles) are difficult to assess with standard radiographs due to the

^a International Weight-Bearing CT Society; ^b Department for Foot and Ankle Surgery Rummelsberg and Nuremberg, Rummelsberg 71, 90592 Schwarzenbruck, Germany; ^c Department of Orthopedics and Rehabilitation, Carver College of Medicine, University of Iowa, 200 Hawkins Dr, Iowa City, IA 52242, USA; ^d Clinique de l'Union, Foot and Ankle Surgery Centre, Boulevard de Ratalens, 31240, Saint-Jean, Toulouse, France; ^e Department of Trauma-, Hand- and Reconstructive Surgery, University Medical Center Hamburg-Eppendorf, Hamburg, Germany; ^f Department of Orthopaedics and Traumatology, University Hospital of Ghent, Corneel Heymanslaan 10, 9000 Gent, Oost-Vlaanderen, België; ^g The Hospital for Special Surgery, 535 East 70th Street, New York, NY 10021, USA

* Corresponding author. Department for Foot and Ankle Surgery Rummelsberg and Nuremberg, Location Hospital Rummelsberg, Rummelsberg 71, Schwarzenbruck 90592, Germany.

E-mail address: martinus.richter@sana.de

superimposition of the different bones.^{1,4} The reason is the "reduction" of a three-dimensional body (foot) to a two-dimensional image (conventional radiograph). Angle measurements with conventional radiographs could be inaccurate due to inaccuracies of the projection (orientation of (central) beam) and/or foot orientation (Fig. 1).^{1,3,5-7} 3D imaging with conventional computed tomography (CT) allows for exact analysis within the 3D data that is not influenced by projection and/or foot orientation but lacks weight-bearing (Fig. 2).^{1,3,4,8} WBCT was introduced 2012 for foot and ankle use as a new technology that allows 3D imaging with full weight-bearing which should be not influenced by projection and/or foot orientation.¹ The cone-beam technology as such is similar to previous applications as for example, intraoperative 3D imaging (Fig. 3).^{3,9} Different devices from different companies became available. Several measurement possibilities had been provided with different software solutions (Tables 1 and 2).¹⁻³ Many clinical application possibilities have been shown.¹⁻³ From the very beginning of the device availability, scientific studies have been used.¹⁻³ Most of the studies investigated the accuracy of the bone position assessment, that is, different measurement of angles between bones or position of bones.¹⁻³ Shortly after, additional measurements as for example, pedography were added.^{10,11} From the previously described parameter, especially the assessment of the hindfoot axis, position of the fibula in relation to the tibia and joint space analysis is important for the assessment of AOA and for treatment planning.

STATUS IN HEALTHY SUBJECTS

The main purpose of WBCT is exact and detailed evaluation of foot and ankle pathologies including alignment and degenerative in natural standing position. However, WBCT can also be used in healthy persons for a better understanding of complex anatomy and biomechanics.^{12,13} Lepojarvi and colleagues investigated the rotational

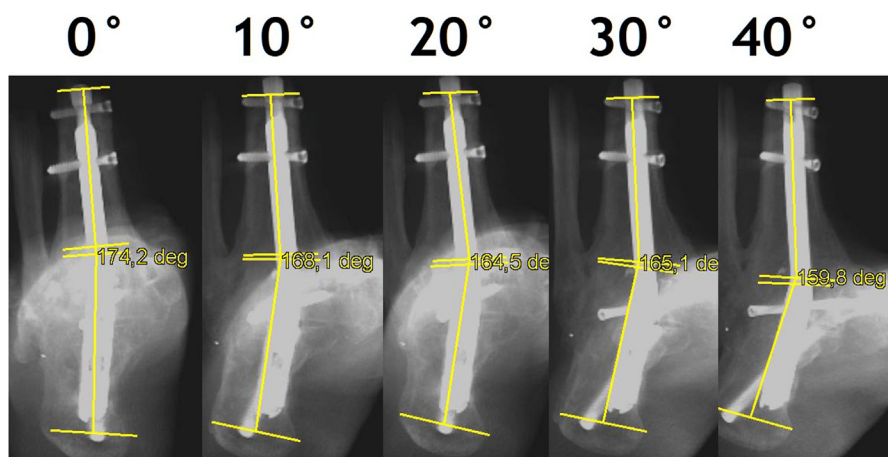


Fig. 1. Conventional radiographs for measurement of hindfoot alignment in a patient with healed tibio-talo-calcaneal arthrodesis with retrograde nail. The healed arthrodesis ensures uniform hindfoot position during repetitive radiographic assessment. Radiographs with different internal rotations (0°–40°) of the foot in relation to the central beam were obtained and the hindfoot angle was measured. The measured hindfoot angles ranged from 5.8° to 21.2°. The different angles are not influenced by the "real" hindfoot angle (healed arthrodesis plus nail) but only by different orientation (internal rotation) of the foot and ankle during radiographic assessment.

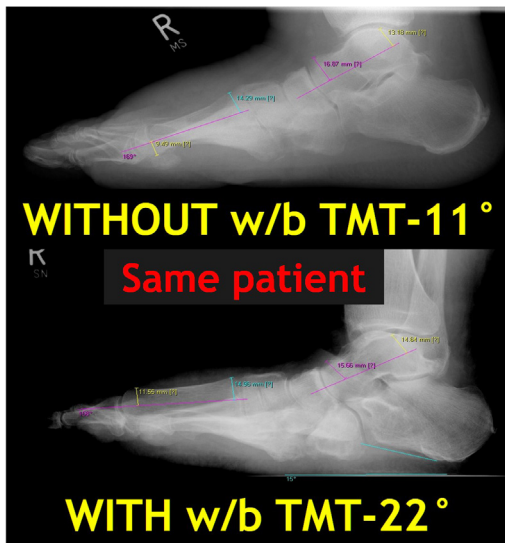


Fig. 2. Lateral radiographs of the right foot from a patient with Charcot arthropathy without weight-bearing (top) and with weight-bearing (bottom). The lateral talo-1st metatarsal-angle (TMT) was measured. This was -11° without and -22° with weight-bearing showing the influence of weight-bearing on the relationship of the bones (angles).

dynamics of the distal tibiofibular joint by analysis of fibula position in axial plane.¹³ In neutrally aligned ankle under weight-bearing conditions, the fibula was found anteriorly in the tibial incisura in 88% of all subjects. Internal and external rotation with a mean moment of 30 Nm resulted in a mean sagittal translation of the fibula of 1.5 ± 1.2 mm and in mean fibula rotation of $3.2 \pm 2.8^\circ$.¹³ In their second study, rotational dynamics of the talus were analyzed in the same healthy subjects.¹³ The rotation of the talus, as well as radiographic alignment of mortise, were measured while standing with versus without rotation. Internal and external rotation resulted in significant changes of talus rotation of $10.0 \pm 5.8^\circ$ with any substantial changes in the medial clear space.¹³ The anatomy and kinematics of the distal tibiofibular syndesmosis have been the subject of several studies recently. Hagemeijer and colleagues analyzed 24 healthy ankles

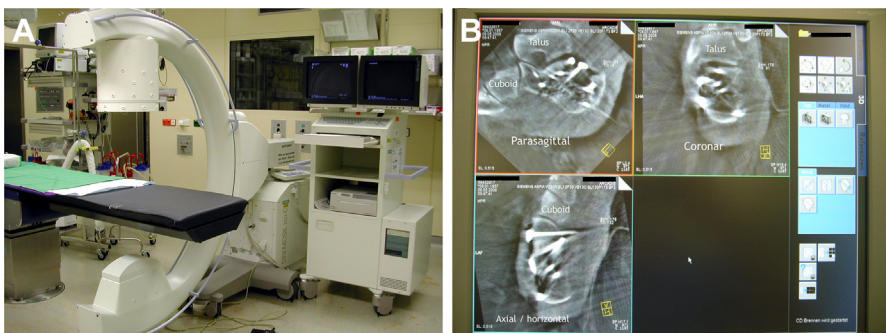


Fig. 3. (A, B) Cone-beam technology application for intraoperative 3D imaging (ISO-C-3D, Siemens, Erlangen, Germany). (A) shows the device in the operating theater and (B) a monitor view example. The monitor shows intraoperative imaging after open reduction and internal fixation of a calcaneal fracture. 3D reformations are shown (parasagittal, top left; coronar, top right; axial, bottom).

Table 1
Radiographic assessment of the forefoot using weight-bearing computed tomography ^{1,56-59}

| Radiographic Measurement | Interobserver Reliability | Intraobserver Reliability | Correlation with Other Measurements | Clinical Findings |
|---|---------------------------|---------------------------|--|--|
| α angle (1st MT pronation angle) | n.a. | n.a. | <ul style="list-style-type: none"> ■ vs. HVA⁵⁵: .076^a, <i>P</i> value < .1 ■ vs. IMA⁵⁵: 144^a, <i>P</i> value < .1 ■ vs. sesamoid position⁵⁵: 019^a, <i>P</i> value < .1 | <ul style="list-style-type: none"> ■ HV group: 21.9°, control group: 13.8°⁵⁵ ● HV group: 8° ± 2° (4°-12°), control group: 2° ± 3° (-4°-8°)² ■ HV group: 17.7° ± 6.9, control group: 14° ± 7.8°⁵⁷ |
| 1st MT/ground angle | n.a. | n.a. | n.a. | <ul style="list-style-type: none"> ● HV group: 18° ± 1°, control group: 21° ± 1°⁵⁶ |
| HVA (2D) | n.a. | n.a. | n.a. | <ul style="list-style-type: none"> ● HV group: 35° ± 3°, control group: 13° ± 4°⁵⁶ ■ HV group: 39.8° ± 8.6°, control group: 14.7° ± 3.1°⁵⁸ ■ HV group: 30.7° ± 8°, control group: 11° ± 3.8°⁵⁷ |
| HVA (3D) | n.a. | n.a. | <ul style="list-style-type: none"> ● vs. HVA on plain radiographs⁵⁶: 95^b, <i>P</i> value < .05 ● vs. HVA (2D)⁵⁶: 94^b, <i>P</i> value < .05 | <ul style="list-style-type: none"> ● HV group: 35° ± 3° (WB), 46° ± 5° (NWB), control group: 15° ± 4° (WB), 32° ± 8° (NWB)⁵⁶ |
| IMA (2D) | n.a. | n.a. | n.a. | <ul style="list-style-type: none"> ● HV group: 19° ± 1°, control group: 11° ± 1°⁵⁶ ■ HV group: 22.2° ± 4.4°, control group: 8.7° ± 1.0°⁴ ■ HV group: 14.6° ± 4.4°, control group: 10.5° ± 2.5°⁵⁷ |
| IMA (3D) | n.a. | n.a. | <ul style="list-style-type: none"> ● vs. IMA on plain radiographs⁵⁶: 72^b, <i>P</i> value < .05 ● vs. IMA (2D)⁵⁶: 81^b, <i>P</i> value < .05 | <ul style="list-style-type: none"> ● HV group: 17° ± 1° (WB), 14° ± 1° (NWB), control group: 11° ± 1° (WB), 8° ± 2° (NWB)⁵⁶ ● 9.3° ± 3.5° (WB), 7.8° ± 3.9° (NWB)⁵⁶ |

| | | | | |
|------------------------------------|------|------|--|--|
| Max. horizontal width (mm) | n.a. | n.a. | n.a. | HV group: 98 ± 1 (WB), 89 ± 2 (NWB), control group: 86 ± 2 (WB), 78 ± 3 (NWB) ⁵⁶ |
| Sesamoid position in coronal plane | n.a. | n.a. | <ul style="list-style-type: none"> ■ vs. α angle.⁵⁵: 019°, P value < .1 ■ vs. HVA.¹: 477°, P value < .01 | <ul style="list-style-type: none"> ■ HV group: true sesamoid subluxation 71.7%, no sesamoid subluxation 28.3%⁵⁵ |
| TMT angle dorsoplantar | n.a. | n.a. | n.a. | <ul style="list-style-type: none"> ● $-5.0^\circ \pm 12.0^\circ$ (WB), $4.3^\circ \pm 10.0^\circ$ (NWB)¹ |
| TMT angle lateral | n.a. | n.a. | n.a. | <ul style="list-style-type: none"> ● $-7.6^\circ \pm 8.2^\circ$ (WB), $0.5^\circ \pm 8.4$ (NWB)¹ |

Abbreviations: HV, hallux valgus; HVA, hallux valgus angle; IMA, intermetatarsal angle; metatarsal, MT; metatarsal, n. a., not available; NWB, non-weight-bearing; TMT, talo-1st metatarsal; WB, weight-bearing.

^a Spearman Rank Correlation Coefficient.

^b Pearson Correlation Coefficient.

Table 2
Radiographic Assessment of the Midfoot and Hindfoot using Weight-Bearing Computed Tomography^{14,22,27,32,45,55,60–62}

| Radiographic Measurement | Interobserver Reliability | Intraobserver Reliability | Correlation with Other Measurements | Clinical Findings |
|--|--|--|-------------------------------------|--|
| Calcaneal pitch angle | n.a. | n.a. | n.a. | ● $17.8^\circ \pm 5.4^\circ$ (WB), $16.5^\circ \pm 5.0^\circ$ (NWB) ⁵⁹ |
| Calcaneofibular distance (mm) | 0.61 ^{a,2} | n.a. | n.a. | ● 0.3 ± 6.0 (WB), 3.6 ± 5.2 (NWB) ² |
| Fibular rotation | n.a. | n.a. | n.a. | ■ syndesmosis injury: $8.4^\circ \pm 7.0^\circ$ ^{27,59} ■ control group: $10.3^\circ \pm 5.5^\circ$ ^{27,59} |
| Foot and ankle offset (%) | 0.99 ± 0.00 ^{c,4} | 0.97 ± 0.02 | n.a. | ● 2.3 ± 2.9 (95%CI: 1.5–3.1) (patients with neutral alignment) ²⁷ ● -11.6 ± 6.9 (95%CI: -13.9 to -9.4) (patients with varus alignment) ²⁷ ● 11.4 ± 5.7 (95%CI: 9.6–13.3) (patients with valgus alignment) ²⁷ |
| HAA | 0.83 ^{a,2} | n.a. | n.a. | ● $21.0^\circ \pm 7.9$ (WB), $19.0^\circ \pm 9.0^\circ$ (NWB) ⁶⁰ ● $10.1^\circ \pm 7.1^\circ$ (WB), $5.4^\circ \pm 5.6^\circ$ (NWB) ⁵⁹ |
| HAA _{CL} | 0.72 (valgus), 0.69 (varus) ^{c,5} | 0.73 (valgus), 0.67 (varus) ⁵ | n.a. | ● 25.2° (valgus), 22° (varus) ⁵ |
| HAA _{LA} | 0.7 (valgus), 0.71 (varus) ^{c,5} | 0.71 (valgus), 0.72 (varus) ⁵ | n.a. | ● 16.4° (valgus), 11.9° (varus) ⁵ |
| HAA _{NOV} | 0.69 (valgus), 0.6 (varus) ^{c,5} | 0.67 (valgus), 0.67 (varus) ⁵ | n.a. | ● 17.7° (valgus), 13.5° (varus) ²² |
| Lateral talocalcaneal joint space width (mm) | 0.82 ^{a,2} | n.a. | n.a. | ● 2.2 ± 1.1 (WB), 2.9 ± 1.7 (NWB) ⁶⁰ |
| Middle facet percentage of uncoverage | 0.75 (0.53–0.87) ⁶ | 0.90 (0.81–0.95) ⁶ | n.a. | ■ 45.3% (AAFD), 4.8% (controls) ³² |

| | | | | |
|--|--|--|---|---|
| Middle facet incongruence angle | 0.93 (0.85–0.96) ⁶ | 0.95 (0.91–0.98) ⁶ | n.a. | ■ 17.3° (AAFD), 0.3° (controls) ³² |
| Naviculocalcaneal distance (mm) | 0.85 ^{a,2} | n.a. | n.a. | ● 15.3 ± 4.7 (WB), 13.5 ± 4.0 (NWB) ⁶⁰ |
| Subtalar inferior facet-horizontal angle | n.a. | n.a. | ■ no correlation with any weight-bearing radiographic measures ⁷ | ■ stage II AAFD group: 15.9° ± 5.7°, control group: 5.7° ± 6.7° ⁴⁵ |
| Subtalar inferior-superior facets angle | n.a. | n.a. | ■ vs AP coverage angle ⁷ : <i>P</i> value .003 ■ vs. AP talar-1st MT angle ⁷ : <i>P</i> value .003 ■ vs. calcaneal pitch ⁷ : <i>P</i> value .014 ■ vs. Meary's angle ⁷ : <i>P</i> value < .001 ■ vs medial column height ⁷ : <i>P</i> value .007 | ■ stage II AAFD group: 21.2° ± 6.7°, control group: 10.7° ± 6.4° ⁴⁵ |
| Subtalar vertical angle | ● 0.975 ^{a,5} ● 0.72 (valgus), 0.73 (varus) ^{c,5} | ● 0.989 ⁸ ● 0.77 (valgus), 0.78 (varus) ⁵ | n.a. | ● 91° (72°-109°) (varus OA group), 109° (97°-120°) (valgus OA group), 98° (85°-114°) (controls) ⁶¹ ● 74.3° (valgus), 69.1° (varus) ⁵ |
| Syndesmosis area | n.a. | n.a. | n.a. | ■ syndesmosis injury: 164.8 ± 46.8 cm ^{3,60} ■ control group: 118.7 ± 37.7 cm ^{14,60} |
| Syndesmosis volume | n.a. | n.a. | n.a. | ■ syndesmosis injury: 5.5 cm ⁶⁰ (3 cm above TP), 14.1 cm ⁶⁰ (5 cm above TP), 33.5 cm ⁶⁰ (10 cm above TP) ⁵⁴ |

(continued on next page)

Table 2
(continued)

| Radiographic Measurement | Interobserver Reliability | Intraobserver Reliability | Correlation with Other Measurements | Clinical Findings |
|------------------------------|--|--|-------------------------------------|---|
| | | | | <ul style="list-style-type: none"> ■ control group: 4.7 cm⁶⁰ (3 cm above TP), 7.9 cm⁶⁰ (5 cm above TP), 23.3 cm⁶⁰ (10 cm above TP)⁵⁴ |
| Talar tilt | 0.92 (valgus), 0.89 (varus) ^{c,5} | 0.89 (valgus), 0.89 (varus) ⁵ | n.a. | <ul style="list-style-type: none"> ● 5.9° (valgus), 4.8° (varus)⁵ |
| Talar translation (mm) | 0.86 (valgus), 0.82 (varus) ^{c,5} | 0.87 (valgus), 0.88 (varus) ⁵ | n.a. | <ul style="list-style-type: none"> ● 21 (valgus), 19 (varus)⁵ |
| Talocalcaneal overlap (mm) | 0.81 ^b | n.a. | n.a. | <ul style="list-style-type: none"> ● 1.4 ± 3.9 (WB), 4.1 ± 3.9 (NWB)⁶⁰ |
| Tibiocalcaneal distance (mm) | 0.72 ^{b,2} | n.a. | n.a. | <ul style="list-style-type: none"> ● 20.6 ± 4.2 (WB), 21.7 ± 6.2 (NWB)⁶⁰ |

Abbreviations: AAFD, adult-acquired flatfoot deformity; AP, antero-posterior; HAA, hindfoot alignment angle; HAA_{CL}, hindfoot alignment angle measured by the bisector of the Achilles tendon and the calcaneus; HAA_{LA}, hindfoot alignment angle measured using an inclination set at 45° to simulate the long axial view; HAA_{NOV}, hindfoot alignment angle measured by combining the inclination of the tibia (anatomic axis) and inclination of the talus and calcaneus (talocalcaneal angle); MT, metatarsal; n.a., not available; NWB, non-weight-bearing; TP, tibial plafond; WB, weight-bearing.

^a Intraclass correlation coefficient to assess the interobserver reliability (measurements of one orthopedic resident, one medical student, and one scientific associate).

^b Intraclass correlation coefficient to assess the interobserver reliability (measurements of 2 musculoskeletal radiologists).

^c Intraclass correlation coefficient to assess the interobserver reliability (measurement of 2 independent observers)

and found the mean fibular sagittal plane position of 1.8 ± 1.0 mm as well as mean fibular rotation of $11.5 \pm 5.2^\circ$.¹⁴ Malhotra and colleagues addressed the effect of weight-bearing on the measurements of the distal tibiofibular syndesmosis.¹⁵ They found that the full weight-bearing resulted in a substantial lateral and posterior sagittal translation as well as external rotation of the distal fibula in relation to the incisura^{15,16}

DEGREE OF ANKLE OSTEOARTHRITIS

The authors propose a four-degree classification AOA for WBCT (Fig. 4) The first degree of AOA includes joint space narrowing but not complete loss and osteophyte formation (see Fig. 4A). The second degree includes partial or complete loss of joint space (see Fig. 4B,C). The third degree includes additional subchondral cysts but remaining joint surface congruency (see Fig. 4D). The fourth degree includes additional joint surface destruction and incongruency (see Fig. 4E,F). This new classification combines the classical signs of osteoarthritis (joint space narrowing or loss, osteophyte formation, and subchondral cysts) with 3D visualization.

ASSESSMENT OF ALIGNMENT

Alignment is a paramount factor in the understanding of AOA, on which WBCT can shed significant new light. With regards to both the preoperative factors which lead



Fig. 4. (A–F). (A) show first degree of osteoarthritis with joint space narrowing but not complete loss and osteophyte formation. (B, C) show second degree of osteoarthritis with partial or complete loss of joint space. (D) shows third degree of osteoarthritis with additional subchondral cysts but remaining joint surface congruency. (E, F) show fourth degree of osteoarthritis with additional joint surface destruction and incongruency.

to the progressive degeneration of cartilage and the postoperative factors which may lead to surgical failure, 3D weight-bearing imaging using cone-beam technology has recently improved our level of understanding with higher quality evidence.^{17–20} The classification of arthritic joint line degeneration based on the thickness of radiolucent cartilage, is complexified by being in 3D and necessitates the development of computerized algorithm such as distance mapping (DM) to provide accurate analysis and quantifiable data.^{20,21} One of the 2 main reasons for this difficulty is our education as surgeons, based on 2D weight-bearing radiographs for measurements and 3D non-weight-bearing CT for details. The new modality of WBCT now replaces both (Fig. 5).

To improve this, several methods have been proposed to:

- 1 Adapt 2D alignment to the new 3D environment by defining reliable 3D landmarks. In this case, the measurement's plane is described based on reliable anatomic landmarks such as the lowest point on the calcaneus tuberosity and the longitudinal tibia axis, or the vertical axis for the coronal and transverse planes (Fig. 6)^{22–24}
- 2 Identify the true 3D angles using computerized methods such as segmentation. In this case, a specialized software is required to perform segmentation (identification of individual bones) of the anatomy (Fig. 7), and 3D measurements.^{23,25}
- 3 Propose a foot ankle offset, which requires identifying 3 landmarks on the weight-bearing plane (foot tripod) and the center of the ankle joint (Fig. 8).^{26–29}

In daily practice, WBCT allows to evaluate alignment in a myriad way. First, a "skin" 3D rendering is possible, combined with digital podoscopy (Fig. 9), allowing for virtual clinical evaluation of hindfoot, ankle orientation, and arch type.³⁰ Second, most WBCT machines provide built in capacity to perform, or reconstruct conventional radiographs (or DRR, standing for digitally reconstructed radiographs) (Fig. 10). Third, the 3 methods listed above may be applied to the 3D dataset, using multiplanar viewing software (Fig. 11).

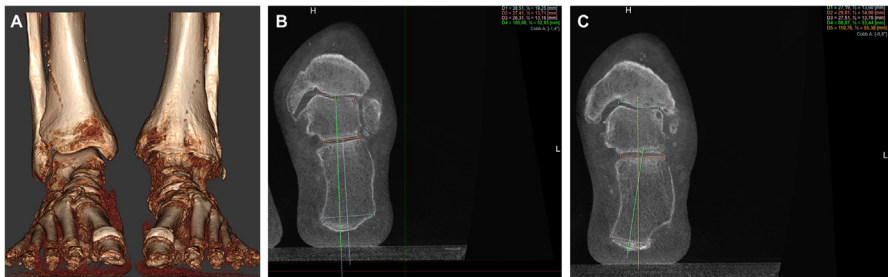


Fig. 5. (A) shows the 3D rendering of the case. In our experience, this advantageously corresponds to a "snapshot" view which allows to have a general overview of the bony architecture before switching to Multi Planar View. In (B), the hindfoot alignment angle was measured while the antero-posterior axis of the scanner was set as the sagittal plane. A 1.4° varus was found. In (C), the axis of the second metatarsal was used as the sagittal reference plane. An 8.8° varus was found. We need to stress here that this does not mean that WBCT is not reliable in terms of measurement: on the contrary, it means that 2D angles which need to be set in a particular plane are not adapted to WBCT because of the choice of this plane, which is not reliable. Angles and distances are not compatible with 3D: they belong to the 2D world.



Fig. 6. (A) shows the sagittal view whereby the coronal plane (represented by the *blue line*) passes through the lowest point of the calcaneus and the center of the ankle joint. In (B), we are looking at the axial view whereby the sagittal plane (represented by the *green lines*) is set along the 2nd metatarsal.

WBCT AND FOOT AND ANKLE OFFSET (FAO) IN THE ASSESSMENT OF THE VALGUS ARTHRITIC ANKLE AS PART OF PROGRESSIVE COLLAPSING FOOT DEFORMITY.

Similarly, WBCT and semiautomatic biometric measurements such as the FAO can also be used in the preoperative and postoperative assessment of the arthritic valgus ankle, providing an idea in regard to the contribution of the ankle and hindfoot malalignment in the overall deformity.^{29,31} WBCT is recommended in the assessment of this complex deformity, and allow proper assessment of the ankle and hindfoot components of the PCFD. Increased preoperative FAO measurements in patients undergoing patients with total ankle replacement (TAR) were found to significantly predict the number of additional realignment procedures, such as calcaneal osteotomies, that were needed to balance the foot and ankle, once the ankle deformity was corrected (Figs. 12 and 13)^{29,32,33}

THREE-DIMENSIONAL MEASUREMENTS IN ANKLE OSTEOARTHRITIS USING WEIGHT-BEARING CONE-BEAM COMPUTED TOMOGRAPHY

Deformity is a critical contributor to the development and progression of ankle OA.^{19,34,35} Two pivotal publications have examined the role of a WBCT specifically in ankle OA using 2-dimensional measurements.^{1,19,34,36–41} Kim and colleagues quantified the rotation of the talus within the mortise of patients with varus ankle OA.⁴² They found a higher internal rotation of the talus than the control group, which altered according to the severity of ankle OA. Krähenbühl and colleagues used a weight-

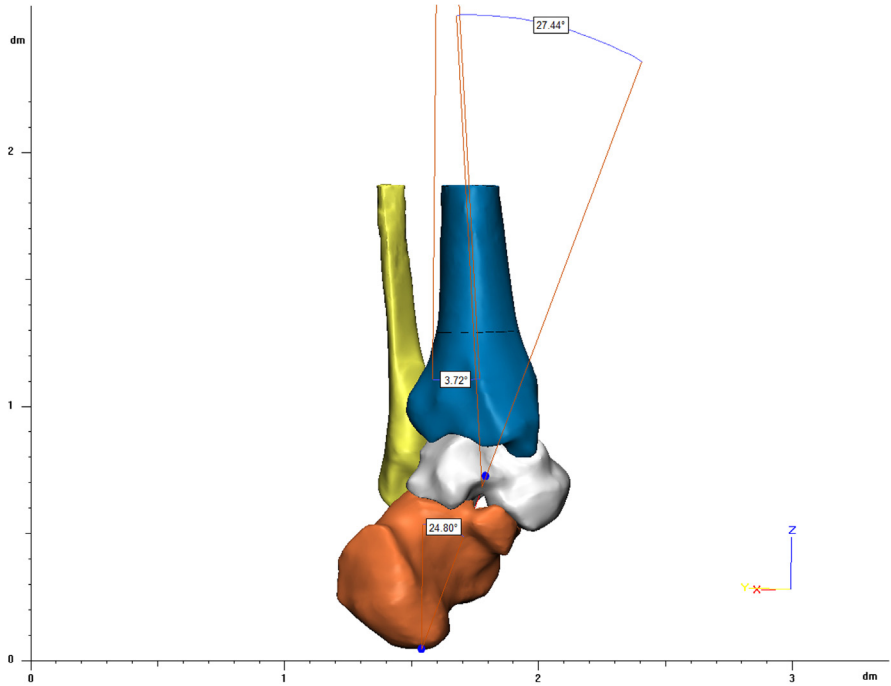


Fig. 7. Shows an example of 3D angles being measured directly using a 3D model created from a patient dataset using manual segmentation (contouring of the bones on each slice).

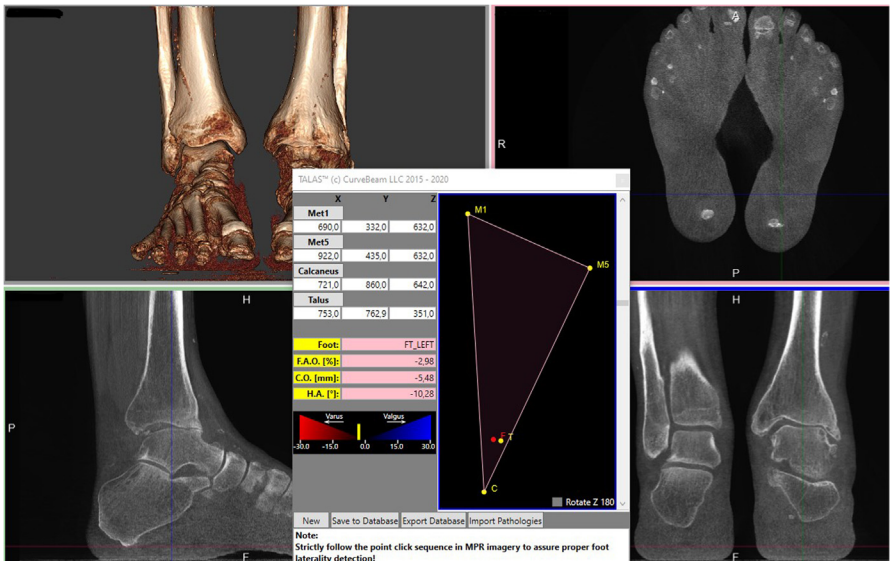


Fig. 8. In the same case as **Fig. 7**, hindfoot alignment is measured using the 3D biometric FAO, via semiautomatic software.



Fig. 9. (A) shows the 3D rendering of the skin view. In (B), the digital podoscopy can be observed.

bearing CT to assess the orientation of the subtalar joint in ankle varus and valgus OA.⁴³ They could demonstrate the compensation of the subtalar joint in varus—but not in valgus ankle OA. The aforementioned studies contained a first characterization of the structural configuration of hindfoot deformities in the presence of physiologic without superposition but remained limited by a 2-dimensional assessment of 3-dimensional deformities. Fortunately, recent software modalities are able to generate 3-dimensional model from weight-bearing CT images. Three studies focused specifically on techniques to translate former 2-dimensional measurements to their



Fig. 10. This shows the DRR automatically generated from the case dataset, on which hind-foot alignment has been manually measured at 4.8° varus.

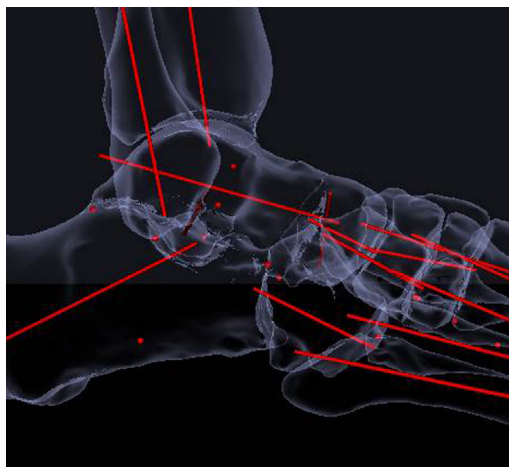


Fig. 11. An example of automatic segmentation of bones and recognition of the principal longitudinal axes.

3-dimensional equivalents using weight-bearing CT (see **Figs. 5** and **6**; **Fig. 14**).^{25,40,44} One of the main advantages of these techniques is the ability of the software to compute different landmarks and axes based on the volumetric properties of the bone models. Geometric functions allow or the centroid for example, of the talus, which is used to calculate the measurements by the software. This overcomes the

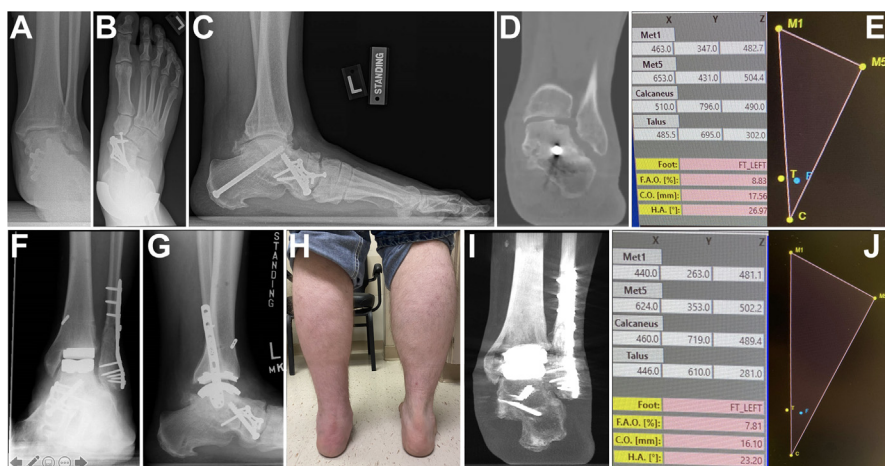


Fig. 12. (A–J) 58-year-old male patient with history of rigid PCFD and prior triple fusion, presenting with symptomatic end-stage ankle arthritis, fixed mild valgus ankle deformity. Preoperative conventional weight-bearing radiographic assessment with Mortise ankle (A), anteroposterior (B) and lateral foot incidences (C) and preoperative WBCT assessment demonstrating mild coronal plane ankle valgus deformity (D) and an FAO of 8.83% (E). Postoperative 6-month conventional weight-bearing radiographic assessment demonstrating well-aligned TAR implants on Mortise (F) and lateral ankle views (G), but with a clinically mild residual asymmetric left hindfoot valgus (H) and WBCT images confirming the residual deformity (I) and still increased FAO of 7.81% (J).

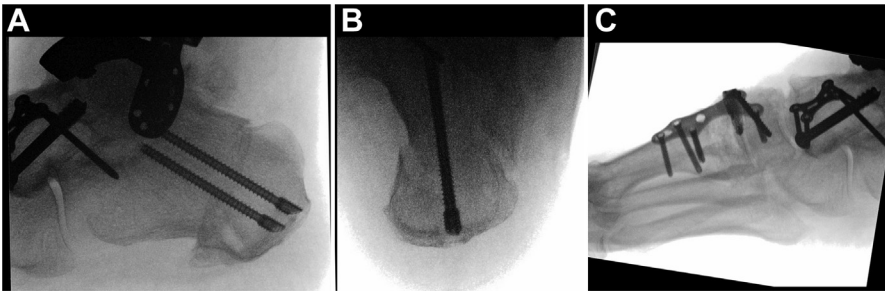


Fig. 13. A–C). Intraoperative fluoroscopic images demonstrating additional surgical realignment procedure in the same patient with a medial displacement calcaneal osteotomy (A, B) and plantarflexion fusion of the first tarsometatarsal joint (C), to realign the foot tripod underneath the ankle.

measurement errors caused by former manual acquisition of the axes or landmarks and is reflected in the higher reliability coefficients associated with 3-dimensional measurements compared with 2-dimensional measurements.²⁴ Moreover, the application of these measurements has demonstrated their relevance in the pre and

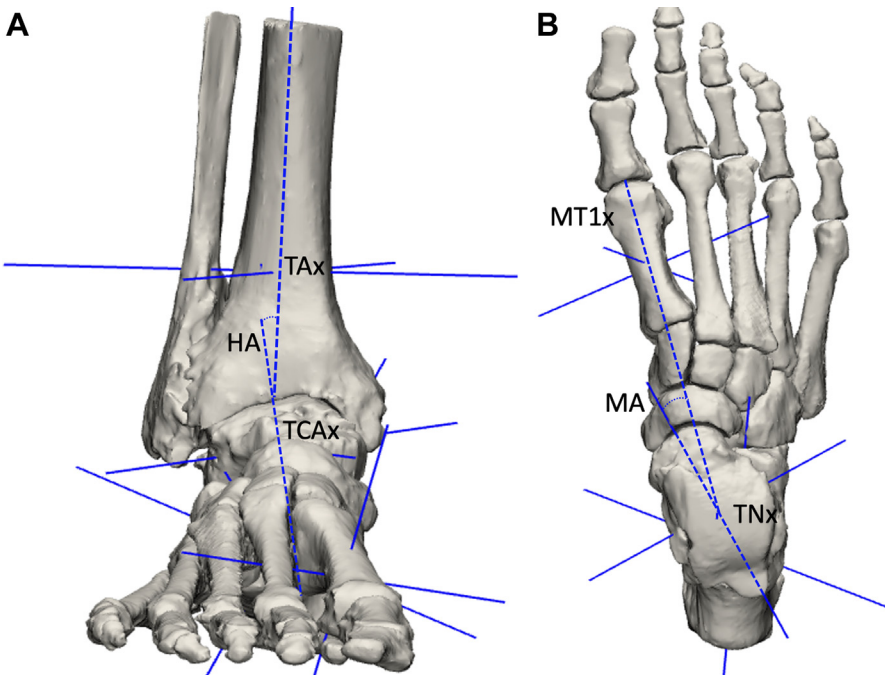


Fig. 14. (A, B). Overview of 3-dimensional measurements in a patient with AOA and varus deformity of the hindfoot. Computed measurements allow to calculate the best fitted axis of the tibia (TAx) and talocalcaneal axis (TCAX) by connecting the calculated most inferior point of the calcaneus and centroid of the talus. The hindfoot angle (HA) in the coronal plane is calculated based on the intersection of the TAx and TCAX (A). The software calculates the best fitted longitudinal axis of the first metatarsal (MT1x) and of the talar neck (TNx). The intersection of the MT1x and TNx constitutes the Méry angle (MA) in the axial plane (B).

postoperative assessment of both valgus and varus hindfoot deformities.^{23,24,45} On the contrary, one of the main disadvantages remains the time consumption to segment each CT-slide separately to generate these models. This remains the main obstacle for their routine use in clinical practice at present. However, advances in the software modalities allow for automatic segmentations of the bony structures, which enabled the first applications of automated measurements.⁴⁶ It is expected that these automated measurements will facilitate the application of 3-dimensional measurement in clinical practice, but future research is still mandatory to confirm the initial promising findings (see Fig. 14).

Deformity Correction with Patient-Specific Guides

Supramalleolar osteotomies are an established treatment option to correct valgus or varus deformity in patients presenting with AOA, most frequently by an opening or closing of osteotomy.^{16,43,47,48} This results in pain relief and improvement of function both on the mid- and long-term follow-up in patients with mild to moderate AOA.^{12,48} This can be attributed to a shift in the weight-bearing axis, which redistributes and mitigates the peak concentration of stress within the ankle.^{49,50} One biomechanical

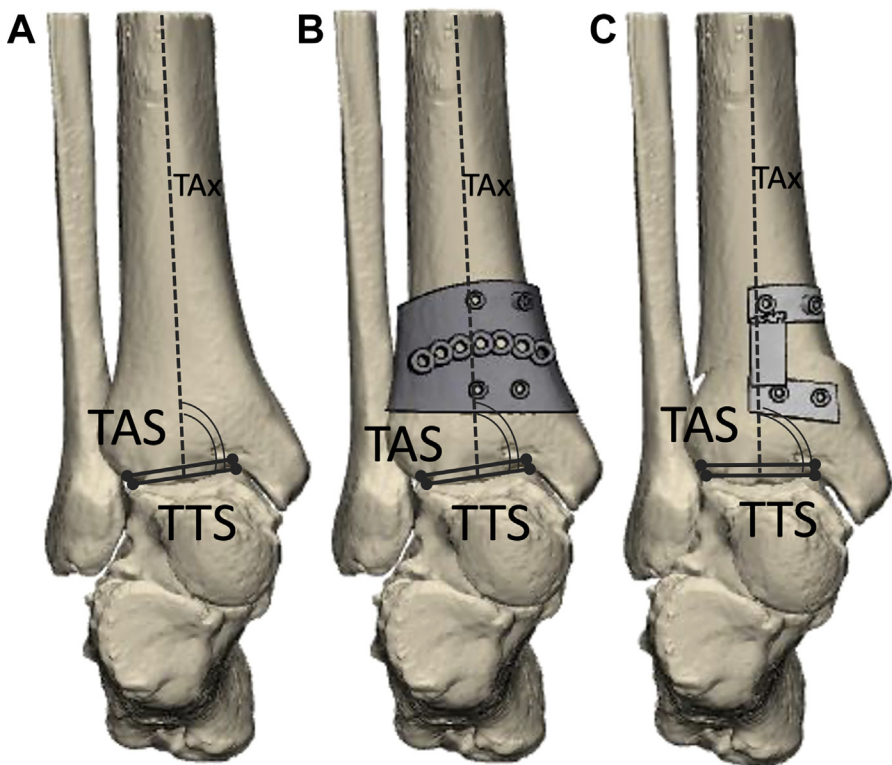


Fig. 15. (A–C). Overview of an ankle varus deformity correction using patient specific guides designed on weightbearing CT imaging. Pre-operative three-dimensional reconstruction of an ankle varus deformity (A) Fitting of the patient specific dome shaped osteotomy guide (B) A second patient specific guide is applied to hold the dome shaped correction of the distal tibia in place prior to a plate and screw osteosynthesis (C). Image courtesy of dr Kris Buedts

disadvantage of the closing or opening wedge osteotomy, is a medialized or lateralized center of the talus.⁴³ This shortcoming can be overcome in congruent ankle varus or valgus deformities by using a dome-shaped supramalleolar osteotomy, which keeps the talus centered under mechanical axis.⁵¹ However, this procedure remains technically demanding to perform free-hand. This technical drawback can be overcome by the use of a patient-specific guide, which has shown to improve the accuracy of corrective osteotomies.¹⁹ Even though the templates were first planned based on conventional CT, the advantages of implementing WBCT imaging to generate patient-specific guides are twofold. First, the correct level of the osteotomy can be determined based on the fit of the guide containing different sleeves to perform the multiple drill hole technique described by Wagner and colleagues⁵² Second, the pre-operative alignment can be determined using the aforementioned 3-dimensional measurements and a virtual correction can be performed until the desired position is achieved (Fig. 15A, B).

On this corrected model a second guide can be designed using the contours of the tibia proximal and distal of the osteotomy (Fig. 15C). During surgery, this second guide indicates the correct amount of rotation after a dome shape osteotomy based on the fit of the tibia proximal and distal of the osteotomy.

The preliminary results of this technique demonstrated a good clinical outcome and accuracy within the 2° of the planned correction. A similar approach can be used in other types of supramalleolar osteotomies, but the potential benefits should be confirmed in long-term and comparative prospective studies.

EFFECT OF ANKLE INSTABILITY

Krähenbühl and colleagues⁵³ established a cadaveric syndesmosis instability model by sectioning of anterior inferior tibiofibular ligament versus deltoid transection.⁴³

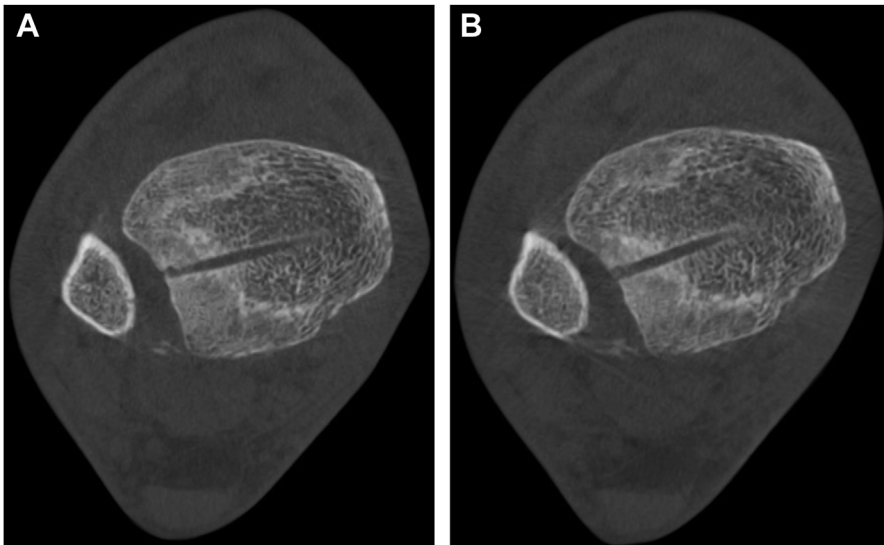


Fig. 16. Preoperative axial weight-bearing CT demonstrating recurrent syndesmosis instability. (A) shows imaging in the neutral position without rotation demonstrates substantial widening of distal syndesmosis. (B) shows that internal rotation results in substantial increase of posterior tibiofibular distance and decrease of anterior tibiofibular distance.



Fig. 17. (A–D) Preoperative (A) bilateral standing anteroposterior ankle (B) Mortise ankle (C) lateral ankle and (D) Saltzman radiographs demonstrating severe right bone-on-bone ankle joint osteoarthritis and bilateral varus deformities of the ankle, right greater than left.

There was no substantial difference in the radiographic assessment of ligamentous syndesmosis instability between weight-bearing and non-weight-bearing conditions. However, torque application has a substantial impact on radiographic syndesmosis assessment using digitally reconstructive radiographs as well as axial WBCT scans (Fig. 16).⁴³ Del Rio and colleagues analyzed 2D syndesmosis area measurements on axial scans in both ankles of 39 patients with syndesmosis injury under weight-bearing versus non-weight-bearing conditions.⁵⁴ As expected, there were significant differences between healthy and injured ankles with $3.4 \pm 6.7 \text{ mm}^2$ versus $16.6 \pm 9.9 \text{ mm}^2$, respectively. Furthermore, injured ankles demonstrated a significantly higher increase in the measured surface between both conditions than non-injured ankles.⁵⁴ Bhimani and colleagues performed 3D volumetric measurements of the distal tibiofibular syndesmosis in 12 patients with unilateral syndesmotic instability.⁵⁵ The volumes were measured 3, 5, and 10 cm above the tibial plafond. At all



Fig. 18. Preoperative weight-bearing CT scan performed with Prophecy (Wright Medical Group, Memphis, TN, USA) protocol to define anatomic and mechanical axes of the ankle is shown. On the sagittal view (A), severe arthritis is noted at the level of the ankle and the corresponding slices of the knee joint are visualized. On the coronal views, the ankle and knee are not seen in the same view, but taken together (B) the severe arthritis of the ankle is noted and (C) the center of the knee joint can be visualized to establish the same axes.



Fig. 19. Intraoperative C-arm fluoroscopic image of right foot showing placement of wire through the prophecy guide (not visible) along the mechanical axis of the tibia.

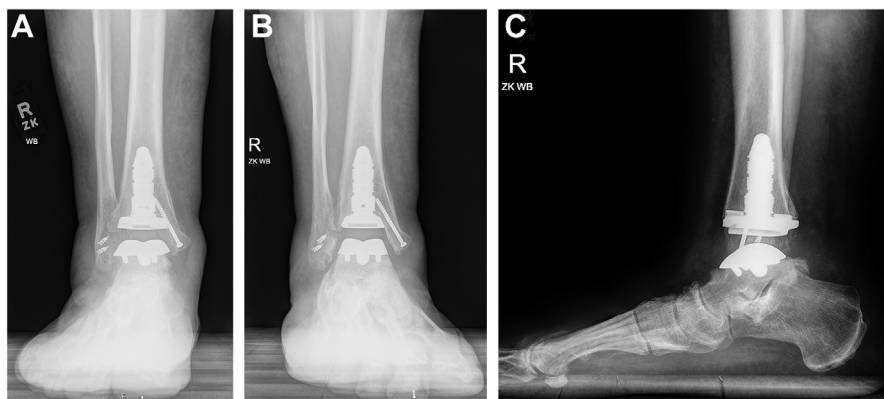


Fig. 20. Postoperative (A) anteroposterior (B) Mortise (C) lateral radiographs of the right ankle demonstrating implantation of INBONE Total Ankle System. A medial malleolus screw has been placed to prophylactically protect the bone and 2 anchors in the fibula have been placed to perform lateral ligament tightening/repair.

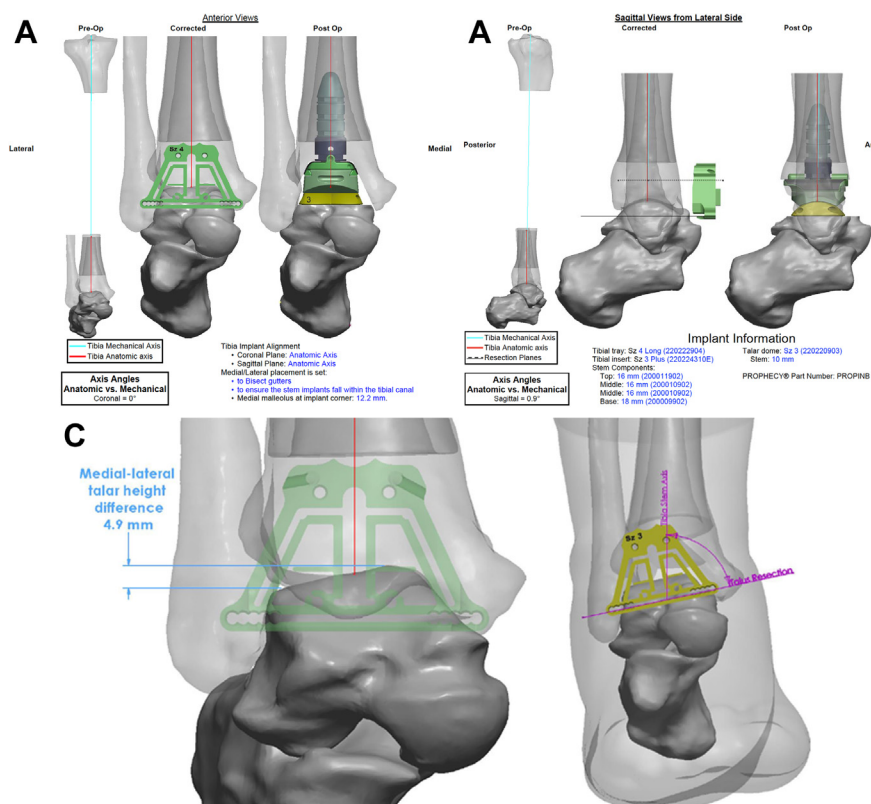


Fig. 21. Images from Prophecy INBONE preoperative navigation guide created based on weight-bearing CT imaging. Anterior view of the guide describing expected tibia implant alignment and medial/lateral placement, as well as angles for anatomic versus mechanical axes (A). Sagittal view from the lateral side describing expected implant sizing, as well as angles for anatomic versus mechanical axes (B). Preoperative medial-lateral talar height difference of 4.9 mm is described (C). The talus resection guide is shown relative to the talar bone and the planned tibia alignment axis, demonstrating expected correction from varus with resections.

3 levels, the measured volume was significantly higher with observed difference of $1.8 \pm 1.4 \text{ cm}^3$, $5.9 \pm 1.9 \text{ cm}^3$, and $9.5 \pm 2.5 \text{ cm}^3$, respectively.⁵⁵

Planning total ankle replacement

WBCT can not only be used to assess hindfoot and ankle alignment and pathology in the setting of ankle arthritis, but it can couple with other developing technology to assist in the surgical planning and performance of total ankle replacement (Figs. 17–21). Now that WBCT can be performed up to the level of the knee or higher, it can be used to identify the anatomic and mechanical axis of the tibia, among other parameters, that can allow the surgeon to place an implant with accurate alignment.

CLINICS CARE POINTS

- Technology of WBCT allows for 3D imaging with weightbearing with low radiation dose
- Evidence of WBCT is high for accuracy and lower for clinical benefit
- Assessment of ankle OA in WBCT provides important information about degree of OA and alignment

DISCLOSURE

M. Richter is a consultant of Curvebeam, Ossio, Geistlich and Intercus, and proprietor of R-Innovation. F. Lintz is consultant of Curvebeam, Follow and Newclip Technics and proprietor of L-Innov. C. de Cesar Netto is a consultant for Curvebeam, Ossio and Paragon 28. A. Barg is a consultant of Medartis, A. Burssens is a consultant of Curvebeam. S. Ellis is a consultant for Paragon 28 and Wright Medical, and currently serves as the President of the AOFAS Foundation. All authors are board member of the International WBCT Society. The International WBCT Society is financially supported by Curvebeam, Carestream, Paragon 28 and Footinnovate.

REFERENCES

1. Richter M, Seidl B, Zech S, et al. PedCAT for 3D-Imaging in Standing Position Allows for More Accurate Bone Position (Angle) Measurement than Radiographs or CT. *Foot Ankle Surg* 2014;20:201–7.
2. Richter MZS, Hahn S. PedCAT for Radiographic 3D-Imaging in Standing Position. *Fuss Sprungg* 2015;13:85–102.
3. Richter M, Lintz F, Cesar de Netto C, et al. Weight bearing cone beam computed tomography (WBCT) in the foot and ankle. A scientific, technical and clinical guide. Cham (Switzerland): Springer Nature Switzerland AG; 2020.
4. Ferri M, Scharfenberger AV, Goplen G, et al. Weightbearing CT scan of severe flexible pes planus deformities. *Foot Ankle Int* 2008;29(2):199–204.
5. Johnson JE, Lamdan R, Granberry WF, et al. Hindfoot coronal alignment: a modified radiographic method. *Foot Ankle Int* 1999;20(12):818–25.
6. Richter M. Computer aided surgery in foot and ankle: applications and perspectives. *Int Orthop* 2013;37(9):1737–45.
7. Richter M. Computer Based Systems in Foot and Ankle Surgery at the Beginning of the 21st Century. *Fuss Sprungg* 2006;4(1):59–71.
8. Kido M, Ikoma K, Imai K, et al. Load response of the tarsal bones in patients with flatfoot deformity: in vivo 3D study. *Foot Ankle Int* 2011;32(11):1017–22.

9. Richter M, Geerling J, Zech S, et al. Intraoperative three-dimensional imaging with a motorized mobile C-arm (SIREMOBIL ISO-C-3D) in foot and ankle trauma care: a preliminary report. *J Orthop Trauma* 2005;19(4):259–66.
10. Richter M, Lintz F, Zech S, et al. Combination of PedCAT Weightbearing CT With Pedography Assessment of the Relationship Between Anatomy-Based Foot Center and Force/Pressure-Based Center of Gravity. *Foot Ankle Int* 2018;39(3):361–8.
11. Richter M, Zech S, Hahn S, et al. Combination of pedCAT for 3D imaging in standing position with pedography shows no statistical correlation of bone position with force/pressure distribution. *J Foot Ankle Surg* 2016;55(2):240–6.
12. Colin F, Horn Lang T, Zwicky L, et al. Subtalar joint configuration on weightbearing CT scan. *Foot Ankle Int* 2014;35(10):1057–62.
13. Lepojarvi S, Niinimäki J, Pakarinen H, et al. Rotational Dynamics of the Normal Distal Tibiofibular Joint With Weight-Bearing Computed Tomography. *Foot Ankle Int* 2016;37(6):627–35.
14. Hagemeyer NC, Chang SH, Abdelaziz ME, et al. Range of Normal and Abnormal Syndesmotic Measurements Using Weightbearing CT. *Foot Ankle Int* 2019;40(12):1430–7.
15. Malhotra K, Welck M, Cullen N, et al. The effects of weight bearing on the distal tibiofibular syndesmosis: A study comparing weight bearing-CT with conventional CT. *Foot Ankle Surg* 2019;25(4):511–6.
16. Krähenbühl N, Akkaya M, Dodd AE, et al. Impact of the rotational position of the hindfoot on measurements assessing the integrity of the distal tibio-fibular syndesmosis. *Foot Ankle Surg* 2020;26(7):810–7.
17. Lintz F, Bernasconi A, Baschet L, et al. Relationship Between Chronic Lateral Ankle Instability and Hindfoot Varus Using Weight-Bearing Cone Beam Computed Tomography. *Foot Ankle Int* 2019;40(10):1175–81.
18. Lintz F, Mast J, Bernasconi A, et al. 3D, Weightbearing Topographical Study of Periprosthetic Cysts and Alignment in Total Ankle Replacement. *Foot Ankle Int* 2020;41(1):1–9.
19. Barg A, Bailey T, Richter M, et al. Weightbearing Computed Tomography of the Foot and Ankle: Emerging Technology Topical Review. *Foot Ankle Int* 2018;39(3):376–86.
20. Lintz F, Jepsen M, De Cesar Netto C, et al. Distance mapping of the foot and ankle joints using weightbearing CT: The cavovarus configuration. *Foot Ankle Surg* 2020;27(4):412–20.
21. Siegler S, Konow T, Belvedere C, et al. Analysis of surface-to-surface distance mapping during three-dimensional motion at the ankle and subtalar joints. *J Biomech* 2018;76:204–11.
22. Burssens A, Peeters J, Buedts K, et al. Measuring hindfoot alignment in weight bearing CT: A novel clinical relevant measurement method. *Foot Ankle Surg* 2016;22(4):233–8.
23. Burssens A, Peeters J, Peiffer M, et al. Reliability and correlation analysis of computed methods to convert conventional 2D radiological hindfoot measurements to a 3D setting using weightbearing CT. *Int J Comput Assist Radiol Surg* 2018;13(12):1999–2008.
24. Burssens A, Van Herzele E, Leenders T, et al. Weightbearing CT in normal hindfoot alignment - Presence of a constitutional valgus? *Foot Ankle Surg* 2018;24(3):213–8.
25. Burssens A, Vermue H, Barg A, et al. Templating of syndesmotic ankle lesions by use of 3D analysis in weightbearing and nonweightbearing CT. *Foot Ankle Int* 2018;39(12):1487–96.

26. Lintz F, Barton T, Millet M, et al. Ground reaction force calcaneal offset: a new measurement of hindfoot alignment. *Foot Ankle Surg* 2012;18(1):9–14.
27. Lintz F, Welck M, Bernasconi A, et al. 3D biometrics for hindfoot alignment using weightbearing CT. *Foot Ankle Int* 2017;38(6):684–9.
28. Zhang JZ, Lintz F, Bernasconi A, et al. 3D Biometrics for Hindfoot Alignment Using Weightbearing Computed Tomography. *Foot Ankle Int* 2019;684–9.
29. de Cesar Netto C, Bang K, Mansur NS, et al. Multiplanar semiautomatic assessment of foot and ankle offset in adult acquired flatfoot deformity. *Foot Ankle Int* 2020;41(7):839–48.
30. de Cesar Netto C, Kunas GC, Soukup D, et al. Correlation of clinical evaluation and radiographic hindfoot alignment in Stage II adult-acquired flatfoot deformity. *Foot Ankle Int* 2018;39(7):771–9.
31. Bluman EM, Title CI, Myerson MS. Posterior tibial tendon rupture: a refined classification system. *Foot Ankle Clin* 2007;12(2):233–49, v.
32. de Cesar Netto C, Godoy-Santos AL, Saito GH, et al. Subluxation of the middle facet of the subtalar joint as a marker of peritalar subluxation in adult acquired flatfoot deformity: a case-control study. *J Bone Joint Surg Am* 2019;101(20):1838–44.
33. de Cesar Netto C, Bernasconi A, Roberts L, et al. Foot alignment in symptomatic national basketball association players using weightbearing cone beam computed tomography. *Orthopaedic J Sports Med* 2019;7(2). <https://doi.org/10.1177/2325967119826081>.
34. Saltzman CL, Hagy ML, Zimmerman B, et al. How effective is intensive nonoperative initial treatment of patients with diabetes and Charcot arthropathy of the feet? *Clin Orthop Relat Res* 2005;435:185–90.
35. Valderrabano V, Leumann A, Rasch H, et al. Knee-to-ankle mosaicplasty for the treatment of osteochondral lesions of the ankle joint. *Am J Sports Med* 2009;37(Suppl 1):105S–11S.
36. Hintermann B, Nigg BM. Influence of arthrodeses on kinematics of the axially loaded ankle complex during dorsiflexion/plantarflexion. *Foot Ankle Int* 1995;16(10):633–6.
37. Knupp M, Schuh R, Stufkens SA, et al. Subtalar and talonavicular arthrodesis through a single medial approach for the correction of severe planovalgus deformity. *J Bone Joint Surg Br* 2009;91(5):612–5.
38. Hayashi K, Tanaka Y, Kumai T, et al. Correlation of compensatory alignment of the subtalar joint to the progression of primary osteoarthritis of the ankle. *Foot Ankle Int* 2008;29(4):400–6.
39. Steel MW 3rd, Johnson KA, DeWitz MA, et al. Radiographic measurements of the normal adult foot. *Foot Ankle* 1980;1(3):151–8.
40. Carrara C, Belvedere C, Caravaggi P, et al. Techniques for 3D foot bone orientation angles in weight-bearing from cone-beam computed tomography. *Foot Ankle Surg* 2020;27(2):168–74.
41. Lintz F, de Cesar Netto C, Burssens A, et al. The value of axial loading three dimensional (3D) CT as a substitute for full weightbearing (standing) 3D CT: Comparison of reproducibility according to degree of load. *Foot Ankle Surg* 2018;24(6):553–4.
42. Kim JB, Yi Y, Kim JY, et al. Weight-bearing computed tomography findings in varus ankle osteoarthritis: abnormal internal rotation of the talus in the axial plane. *Skeletal Radiol* 2017;46(8):1071–80.
43. Krahenbuhl N, Siegler L, Deforth M, et al. Subtalar joint alignment in ankle osteoarthritis. *Foot Ankle Surg* 2019;25(2):143–9.

44. Lintz F, Welck M, Bernasconi A, et al. 3D Biometrics for Hindfoot Alignment Using Weightbearing CT. *Foot Ankle Int* 2017;38(6):684–9.
45. Cody EA, Williamson ER, Burket JC, et al. Correlation of Talar Anatomy and Subtalar Joint Alignment on Weightbearing Computed Tomography With Radiographic Flatfoot Parameters. *Foot Ankle Int* 2016;37(8):874–81.
46. Kvarda P, Heisler L, Krähenbühl N, et al. 3D Assessment in Posttraumatic Ankle Osteoarthritis. *Foot Ankle Int* 2020;42(2):200–14.
47. Pagenstert GI, Hintermann B, Barg A, et al. Realignment surgery as alternative treatment of varus and valgus ankle osteoarthritis. *Clin orthopaedics Relat Res* 2007;462:156–68.
48. Krähenbühl N, Horn-Lang T, Hintermann B, et al. The subtalar joint: A complex mechanism. *EFORT Open J Rev* 2017;2(7):309–16.
49. Tanaka T, Takeda H, Izumi T, et al. Age-related changes in postural control associated with location of the center of gravity and foot pressure. *Phys Occup Ther Geriatr* 1997;15(2):1–14.
50. Lee DC, de Cesar Netto C, Staggars JR, et al. Clinical and radiographic outcomes of the Kramer osteotomy in the treatment of bunionette deformity. *Foot Ankle Surg* 2018;24(6):530–4.
51. Wagner P, Colin F, Hintermann B. Distal Tibia Dome Osteotomy. *Techn Foot Ankle Surg* 2014;13(2):103–7.
52. Wagner UA, Sangeorzan BJ, Harrington RM, et al. Contact characteristics of the subtalar joint: load distribution between the anterior and posterior facets. *J Orthop Res* 1992;10(4):535–43.
53. Krähenbühl N, Lenz AL, Lisonbee RJ, et al. Morphologic analysis of the subtalar joint using statistical shape modeling. *J Orthop Res* 2020;38(12):2625–33.
54. Del Rio A, Bewsher SM, Roshan-Zamir S, et al. Weightbearing Cone-Beam Computed Tomography of Acute Ankle Syndesmosis Injuries. *J Foot Ankle Surg* 2020;59(2):258–63.
55. Bhimani R, Ashkani-Esfahani S, Lubberts B, et al. Utility of Volumetric Measurement via Weight-Bearing Computed Tomography Scan to Diagnose Syndesmotic Instability. *Foot Ankle Int* 2020;41(7):859–65.
56. Kim Y, Kim JS, Young KW, et al. A new measure of tibial sesamoid position in hallux valgus in relation to the coronal rotation of the first metatarsal in CT Scans. *Foot Ankle Int* 2015;36(8):944–52.
57. Collan L, Kankare JA, Mattila K. The biomechanics of the first metatarsal bone in hallux valgus: a preliminary study utilizing a weight bearing extremity CT. *Foot Ankle Surg* 2013;19(3):155–61.
58. Mahmoud K, Metikala S, Mehta SD, et al. The role of weightbearing computed tomography scan in hallux valgus. *Foot Ankle Int* 2020;42(3):287–93.
59. Kimura T, Kubota M, Suzuki N, et al. Weightbearing computed tomography and 3-Dimensional analysis of mobility changes of the first ray after proximal oblique osteotomy for hallux valgus. *Foot Ankle Int* 2020;42(3):333–9.
60. Richter M, Zech S, Hahn S. PedCAT for radiographic 3D-imaging in standing position. *Fuss Sprungg* 2015;13(2):85–102.
61. Hirschmann A, Pfirrmann CW, Klammer G, et al. Upright cone CT of the hindfoot: comparison of the non-weight-bearing with the upright weight-bearing position. *Eur Radiol* 2014;24(3):553–8.
62. Krahenbuhl N, Tschuck M, Bolliger L, et al. Orientation of the subtalar joint: measurement and reliability using weightbearing CT scans. *Foot Ankle Int* 2016;37(1):109–14.